Probing hierarchical structure formation with a cosmological N-body simulation

AST4320 Numerical project

Candidate number 15003
Institute of Theoretical Astrophysics, University of Oslo
(Dated: November 2025)

In this project, we perform a cosmological N-body simulation to investigate hierarchical structure formation in a Planck ΛCDM Universe. Initial conditions are generated at $z = 127$ using `MUSIC`, evolved to $z = 0$ with `GASOLINE2`, and analysed at seven snapshots spanning $z \simeq 5$ to $z = 0$. We examine the halo mass function and its evolution, finding strong agreement with Press-Schechter predictions ($r \sim 0.95$, $p \lesssim 10^{-4}$). The systematic migration of simulated halos to higher masses with decreasing redshift demonstrates bottom-up hierarchical growth. Internal density profiles of the most massive halos exhibit cuspy NFW profiles with logarithmic slopes $\alpha \to -1$ at small radii and $\alpha \to -3$ at large radii, consistent with collisionless dark matter predictions. Comparison with five independent realisations reveals cosmic variance effects, with higher variance at low halo masses and systematic biases in small-volume simulations. Our results provide compelling evidence for hierarchical structure formation across multiple observables.

I. INTRODUCTION

Understanding how cosmic structures form and evolve is a fundamental goal of modern cosmology. The ΛCDM model predicts that structure grows hierarchically through gravitational instability, where small-scale density perturbations collapse first and merge over time to form progressively larger structures. N-body simulations provide a powerful tool for testing these predictions by following the gravitational evolution of dark matter particles from the early Universe to the present day.

In this project, we perform a cosmological N-body simulation to investigate hierarchical structure formation in a Planck ΛCDM Universe. We generate initial conditions at $z = 127$ using `MUSIC`, evolve the system to $z = 0$ using the `GASOLINE2` code, and analyse the results at seven snapshots corresponding to redshifts $\mathcal{Z} = \{4.933, 4.055, 2.984, 2.029, 1.010, 0.497, 0.000\}$. Dark matter halos are identified using the `AHF` halo finder.

Our analysis focuses on three main objectives. First, we examine the halo mass function and its evolution from high to low redshift, comparing our results with theoretical predictions from the Press-Schechter formalism. Second, we investigate the internal density profiles of identified halos, testing whether they follow the universal Navarro-Frenk-White profile. Finally, we assess cosmic variance by comparing our simulation with five other independent realisations of the same cosmological model, as well as a larger, higher-resolution simulation.

II. THEORY

To analyse the simulated density fields and study structure formation, we introduce the theoretical framework necessary for comparing our results with ΛCDM predictions and the literature. Section II A covers the Press-Schechter formalism and the halo mass function, while Section II B presents the Navarro-Frenk-White profile for analyzing dark matter halo densities.

A. HMF in the Press-Schechter formalism

The Press-Schechter (PS) formalism was the first major attempt to connect the statistics of a Gaussian random density field to the observed statistics of galaxies. We will therefore analyse the simulation data through the lense of the PS formalism since it is the simplest. Specifically, we will compare the number density of halos at different mass scales in our simulation to the *halo mass function* (HMF) derived in the PS theory.

The PS formalism is based on three key assumptions, namely [1]:

1. that the density field contrast δ evolves linearly at all times such that $\delta \propto a$, i.e. proportional to the scale factor;

2. collapse is defined as the moment the linearly extrapolated density fluctuation of a region first crosses the critical value $\delta_c = 1.69$;

3. the probability that a mass at position $\mathbf{x}$ is part of a collapsed object with mass $> M$ is given by

$$P(> M) = P(\delta(\mathbf{x}) > \delta_c \mid M),$$

where P is the probability density function (PDF) of the density field contrast $\delta(\mathbf{x})$ smoothed over a scale corresponding to a mass scale M.

It can be shown (e.g. in the lecture notes of AST4320 [1]) that these assumptions, when applied to a Gaussian random density field with variance $\sigma^2(M)$ after smoothing over the mass scale M, lead to the PDF

$$P(> M) = 1 - \mathrm{erf}\left(\frac{\delta_c}{\sqrt{2}\sigma(M)}\right),$$

where erf(x) is the error-function. Assuming ergodicity, this probability will also correspond to the fraction of mass in the Universe that is part of collapsed structures at this mass scale.

From this, we can derive the HMF which gives the number density of DM halos with mass M

$$\begin{aligned} n(M) &= \frac{\rho_{\mathrm{m}}}{M^2}\sqrt{\frac{2}{\pi}}\exp\bigl(-\nu^2/2\bigr)\nu\left|\frac{\partial\log\sigma}{\partial\log M}\right| \\ &\propto M^{\frac{N-9}{6}}\exp\bigl(-\nu^2/2\bigr). \end{aligned}$$

Here we define $\nu \equiv \delta_c/\sigma(M)$ and ρ_{m} refers to the matter density. The proportionality in the second line is derived from the observed proportionality relation $\sigma^2(M) \propto M^{-\frac{N-3}{3}}$ in which N ranges from ~ -3 at small scales, to ~ 1 at large scales.

In the analysis, we will consider the derived quantity $\mathrm{d}n(M)/\mathrm{d}\log M$, i.e. the number density per unit mass.

B. Navarro-Frenk-White density profile

When we look at the density profiles of the halos present in the simulation during our analysis, we want to check if they follow the Navarro-Frenk-White (NFW) profile. This density profile, first discovered by Navarro, Frenk and White (1996) [2], describes the seemingly "universal" profile followed by simulated CDM halos which has the form

$$\rho_{\mathrm{NFW}}(r) = \frac{\rho_0}{\frac{r}{r_s}\Bigl(1+\frac{r}{r_s}\Bigr)^2}$$

Here, ρ_0 is the *normalisation parameter* which sets the overall normalisation of the density of the halo, and r_s is the so-called *scale radius* which measures the extent of the "core" of the halo.

In the analysis, we will compare the slopes of the simulated DM density profiles in log-space to that of the NFW profile. The expected NFW profile goes as [1]

$$\rho_{\mathrm{NFW}} \propto \begin{cases} r^{-1} & r \ll r_s \\ r^{-3} & r \gg r_s \end{cases},$$

which means that we have to check if the logarithmic slope $\alpha \equiv \mathrm{d}\ln\rho/\mathrm{d}\ln r$ tends to -1 at small r and towards -3 for large radii.

III. METHODS

In this section, we cover the numerical methods used to perform the N-body simulation. Section III A explains the cosmological parameters we used, while Section III B outlines the three stages of the simulation. FInally, we state the numerical tools that were used in the analysis of the data.

A. Cosmological framework

For our simulation, we need to choose a suitable set of cosmological parameters for the calculations. The familiar Planck cosmology was assumed in our case and thus we take the density parameters $\Omega_{\mathrm{m}} = 0.3077$, $\Omega_{\mathrm{b}} = 0.0484$, and $\Omega_\Lambda = 0.6923$. From these parameters we can fint the DM density parameter $\Omega_{\mathrm{DM}} = \Omega_{\mathrm{m}} - \Omega_{\mathrm{b}} = 0.2593$. Note that the sum of the density parameters is one, and the simulation is thus performed for a spatially flat Universe. The Hubble parameter was also set to $H_0 = 67.81$ km/s/Mpc.

From these cosmological parameters, we can find the mass of one DM particle inside the simulation box. The box has sidelength $\ell_{\mathrm{b}} = 20$ Mpc and constains $\mathcal{N} = 64^3 = 262\ 144$ dark matter particles, so the DM mass per particle is then

$$M_{\mathrm{p}} = \frac{\rho_{\mathrm{DM}}\ell_{\mathrm{b}}^3}{\mathcal{N}},$$

where $\rho_{\mathrm{DM}} = \Omega_{\mathrm{DM}}\rho_c$ is the average DM density in the box at $z = 0$. The critical density is given by $\rho_c = 3H_0^2/8\pi G$, whence the particle mass expression can be recast into

$$M_{\mathrm{p}} = \frac{3H_0^2\Omega_{\mathrm{DM}}\ell_{\mathrm{b}}^3}{8\pi G\mathcal{N}} \simeq 1.01\times 10^9 M_\odot.$$

In order for a halo to be resolved, it needs to contain at least 32 DM particles. Thus, the minimum halo we can resolve in our simulation has a mass of around $32M_{\mathrm{p}} \simeq 2.191\times 10^{10} M_\odot$.

B. Simulation

The simulation was performed in three main stages. First, initial conditions (ICs) were generated at a redshift of $z = 127$ using `MUSIC` (Multi-scale initial conditions)[3]. These conditions were then evolved to the present day ($z = 0$) using the TreeSPH code `GASOLINE2` [4]. Finally, DM halos were identified, along with their physical properties, in snapshots corresponding to seven distinct redshifts with the AMIGA Halo Finder (`AHF`)[5].

1. *Generating initial conditions with MUSIC*

The N-body simulation was initialised within a periodic box of sidelength $\ell_{\mathrm{b}} = 20$ Mpc, containing $\mathcal{N} = 64^3$ dark matter particles inside it. This was achieved by giving the dimensions of the box, the number of particles and the cosmological parameters stated in Section III A to the cosmological IC generator `MUSIC`, as well as choosing a random seed. The complete technical methodology for IC generation in `MUSIC` is complex and beyond the scope of the curriculum in AST4320. This section will therefore only focus on the foundational principles, omitting more specialized implementation details, as outlined in the paper by Hahn and Abel [3].

`MUSIC` generates a so-called "nested grid" inside the simulation box, allowing higher resolution for zoom-in simulations, containing the $\mathcal{N}$ dark matter particles. It assumes the collection of particles behaves like a fluid and uses Lagrangian perturbation theory to describe the evolution of the density perturbations in the rest-frame of said fluid. Let the positions and velocities of these fluid elements (particles) be given by

$$\mathbf{x}(t) = \mathbf{q} + \mathbf{L}(\mathbf{q}, t) \quad \text{and} \quad \dot{\mathbf{x}}(t) = \frac{\mathrm{d}}{\mathrm{d}t}\mathbf{L}(\mathbf{q}, t) \ ,$$

where $\mathbf{q}$ is the initial position of the element and $\mathbf{L}$ is the *displacement field*. To first order in the pertubations, the displacement field can be expressed as

$$\mathbf{L}(\mathbf{q}, t) = -\frac{2}{3H_0^2 a^2 D_+(t)} \nabla_{\mathbf{q}} \phi(\mathbf{q}, t),$$

where $D_+(t)$ is the growth factor of linear density perturbations, and ϕ is the gravitational potential which obeys the Poisson equation

$$\nabla_{\mathbf{q}}^2 \phi(\mathbf{q}, t) = \frac{3}{2} H_0^2 a^2 \delta(\mathbf{q}, t).$$

The right hand side of this Poisson equation depends on the density contrast field δ, so to solve for the initial particle positions and velocity fields, we need an initial δ. The initial density contrast is sampled from a GRF distribution, since the model assumes the cosmological principle of homogeneity and isotropy.

From the initial GRF density contrast field, the IC generator solves the Poisson equation iteratively over the nested grids and solves for the initial displacement field, giving us the initial particle positions and velocities.

2. *Simulating using GASOLINE2*

The system was evolved from the initial conditions to the present epoch ($z = 0$) using the `GASOLINE2` N-body code. The gravitational forces are computed using a tree method, and the state of the system is saved in 128 snapshots across the redshift range $127 \geq z \geq 0$.

The code units set the gravitational constant $G = 1$ and normalises density to the critical density $\rho_c = 1$. We therefore get

$$H_0 = \sqrt{\frac{8\pi G \rho_c}{3}} = \sqrt{\frac{8\pi}{3}} \simeq 2.8944$$

for the Hubble parameter in simulation units. Three other conventions are also followed:

1. the simulation box has sidelength $L = 1$;
2. lengths and velocities are comoving;
3. velocities are peculiar from the Hubble flow.

The total mass inside the simulation volume is given by $\rho_\mathrm{m}/\rho_c = \Omega_\mathrm{m}$ in code units. From a similar calculation to the one we did for the particle mass in Section III A, we know that the total physical mass inside the volume is given by

$$M_\mathrm{tot} = \frac{3H_0^2 \Omega_\mathrm{m} \ell_\mathrm{b}^3}{8\pi G} \simeq 3.1414 \times 10^{14} M_\odot,$$

so the convertion factor from code units, to physical units, expressed in solar mass units $M_\odot$, can be calculated as

$$\texttt{dMsolUnit} \equiv \frac{M_\mathrm{tot}}{\Omega_\mathrm{m} M_\odot} \simeq 1.02095 \times 10^{15}$$

3. *AHF: identifying halos*

Once we have the data from the `Gasoline` simulation, we run `AHF` (AMIGA Halo Finder [5]) for the seven different snapshots corresponding to the considered redshifts. This allows us to identify the resolved DM halos in each snapshot and their properties.

C. Analysis tools

To analyse the results from the N-body simulation, we use `pynbody` [6] to extract the data from the `GASOLINE2` and `AHF` files, as well as the stastical methods available in `scipy` and `numpy`. For all visualisations, `matplotlib` was used to generate the figures.

IV. RESULTS

This section presents the key results of our N-body simulations, tracing the growth of cosmic structure from the large-scale density field down to the properties of individual DM halos. In Section IV A, we begin by examining the visual evolution of the cosmic web, from a homogeneous density field at high redshift to a network of filaments and underdense regions at $z = 0$. We then quantify this structure by analyzing the HMF and its evolution in Section IV B. Finally, we zoom in to study the internal density profiles of the most massive halos in Section IV C, before analysing the cosmic variance in Section IV D.

A. Column density maps of the simulation box

We start by looking at the evolution of the DM density in the simulation box as from redshift $z \simeq 5$ to $z = 0$. Figure A1 shows the column density maps for DM projected along the z-axis, i.e. in the (x, y)-plane, for the redshifts in $\mathcal{Z}$, in seperate panels side by side such that we can easily see the evolution over redshift. As we approach $z = 0$, we remark the presence of more and more overdense, as well as underdense, regions in the DM field. At $z = 4.933$, the DM density field starts off as a fairly homogeneous "soup" without much structure. Then over time (decreasing redshift), we start to resolve an increasing number of more massive DM halos that are connected by cosmic filaments. At $z = 0$, we can also observe large underdense regions in the space between the filaments.

B. Halo mass functions

In Figure A2, we show the HMF from the simulation at the redshifts in $\mathcal{Z}$, in which the DM halos have been binned into 50 mass bins in the range $M \in [10^{10}, 10^{15}]$ $M_\odot h^{-1}$. The theoretical Press-Schechter HMF at each redshift has also been plotted underneath the simulation HMF for comparison. The Pearson correlation coefficient and its corresponding p-value was also calculated to check the correlation between the simulation and the theoretical HMF. Their values are indicated in the upper right corner of each panel.

A clear evolutionary pattern is evident in the HMF plots. With decreasing redshift, the simulated data points migrate down the theoretical PS curve, tracking the progression of halos into higher mass ranges. This "sliding" motion is driven by the gravitational accretion of mass onto halos over time.

C. Evolution of the most massive halos

Now we "zoom in" and turn our attention to the evolution of the individual DM halos. In this section, we will therefore take a look at the evolution of the most massive DM halo in the simulation box over redshift, before studying the density profiles of the 10 largest halos.

In Figure 1, we can observed the outline of the most massive DM halo present in the simulation box at three different redshifts, specifically $z = 2.029,\ 1.010,\ 0$, drawn on top of the density image of the halo at $z = 0$. The regions inside the contours correspond to where the DM density exceeds the density at the halo's virial radius $R_{\rm vir}$ as given by the NFW profile fitted to the simulated halo DM density profile. This definition of the halo's spatial extent was chosen for its straightforward implementation.

We observe that the extent of the largest DM halo shrinks with redshift, this indicates that the halo experiences gravitational collapse over time so that the enclosed mass concentrates near the center of the halo, increasing the density while shrinking the virial radius.

In Figure 2, we see the density profiles averaged over the 10 most massive halos at each redshift in $\mathcal{Z}$. The profiles were computed using 40 logarithmically spaced bins in the radial direction. We notice that the main differing feature between the profiles at different redshift can be found at low radii. In fact, for lower redshifts, the curve flattens out faster towards the center ($r \lesssim 10^{-1}R_{\rm vir}$). Qualitatively they look similar to the NFW profile, so a fit of the profiles to the NFW were performed, and the resulting NFW parameters are tabulated in Table I. We notice that the average ρ_0 shows a slight tendency to increase with decreasing redshift. The average scale radius r_s is located at around $0.2R_{\rm vir}$ for all redshifts, while the average concentration (the ratio between the outer radius of the and the scale radius r_s of the halo) ranges from 3.388 to 6.475 with no discernable pattern.

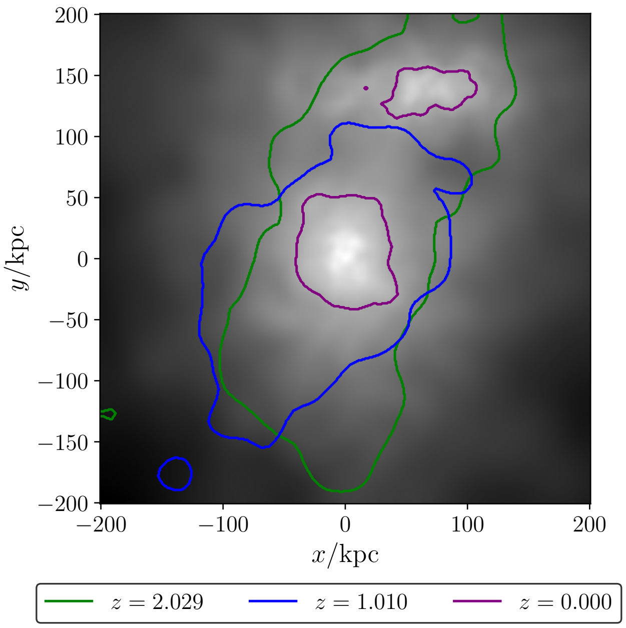

FIG. 1. The outlines of the most massive halos present in the snapshots at redshift $z = 2.029$, $z = 1.010$ and $z = 0.000$, laid on top of the image of the density field of the most massive halo at $z = 0.000$.

To check if the average density profiles match the theoretical NFW profile, we can take a look at the average logarithmic slopes α, which is shown in Figure 3. At low radii, we can clearly see that $\alpha \to -1$, while at large radii, the slope goes to -3 (ignoring the outlier at $z = 2.984$). Both of these features match the predictions of from the NFW profile, as discussed in Section II B.

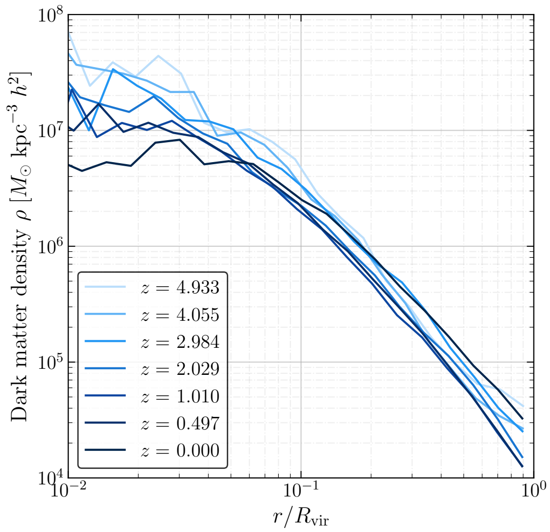

FIG. 2. DM halo density profiles averaged over the 10 most massive halos at each redshift.

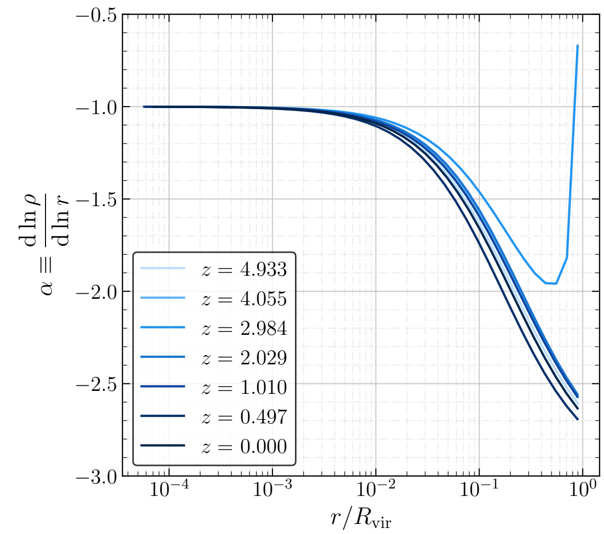

FIG. 3. The logarithmic slopes α averaged over the 10 most massive DM halos at each redshift.

Average NFW parameters			
Redshift	ρ_0 $[M_\odot$ **kpc**$^{-3}$ $h^2]$	$r_s/R_{\rm vir}$	**Concentration**[1]
$z = 4.933$	7.527×10^5	0.2234	4.842
$z = 4.055$	6.034×10^5	0.2493	4.35
$z = 2.984$	undefined[2]	0.1421	3.388
$z = 2.029$	6.159×10^5	0.257	4.23
$z = 1.010$	1.015×10^6	0.2506	4.697
$z = 0.497$	2.435×10^6	0.1631	6.475
$z = 0.000$	4.05×10^6	0.2029	5.487

TABLE I. The average values (over the 10 most massive halos in the snapshot) for the NFW normalisation parameter ρ_0, the scale radius noramlised to the virial radius $r_s/R_{\rm vir}$, and the concentration for each redshift.

D. Cosmic variance

The last thing we consider, is the variance of our simulation results. Five other identical simulations (initialised with $\ell_{\rm b} = 20$ Mpc and $\mathcal{N} = 64^3$) were realised, with different seeds for the IC, by fellow students[3]. A larger, higher resolution, simulation was also performed by our professor, initialised with $\ell_{\rm b} = 40\,$Mpc and $\mathcal{N} = 128^3$. In Figure 4, we see the HMF at $z = 0$ for all of the seven simulations gathered in the left panel. The right panel shows the variance of the seven datapoints at each mass bin.

While we observe that all seven simulations roughly follow the PS halo mass function, the six smaller-volume realisations of the model diverge from the theoretical HMF for $M \lesssim 10^{11} M_\odot h^{-1}$, where they exhibit a systematic deficit in DM halos compared to the expectation from PS theory, and for $M \gtrsim 5 \times 10^{12} M_\odot h^{-1}$, where we observe a greater number density than expected. This bias is mitigated in the larger simulation, which aligns with the PS HMF more accurately across the mass range.

We can also notice that the variance in the data decreases with higher mass. This indicates that the number densities of smaller halos varies more between different realisations of the simulations, while they predict similar number densities for larger halos.

V. DISCUSSION

A. Hierarchical structure formation

The simulation results clearly show the signature of hierarchical structure growth. We observe this in the HMF plots, where the simulated data points migrate down the theoretical PS curve with decreasing redshift, tracking the progression of halos into higher mass bins over time. This "sliding" motion indicates that lower-mass halos form first and are subsequently assembled into more massive systems. Furthermore, the large scale column

[1] The "concentration" is the ratio between the outer radius of the and the scale radius r_s. It is therefore a measure of how big the core is compared to the halo as a whole.

[2] The scale radius r_s is defined as the radius at which $\alpha = -2$. For some strange reason, the slope of the average profile at $z = 2.984$ never reaches -2 (as discussed in Section V B), and the average scale radius is thus undefined.

[3] Candidate numbers: 15001, 15002, 15004, 15008 and 15012

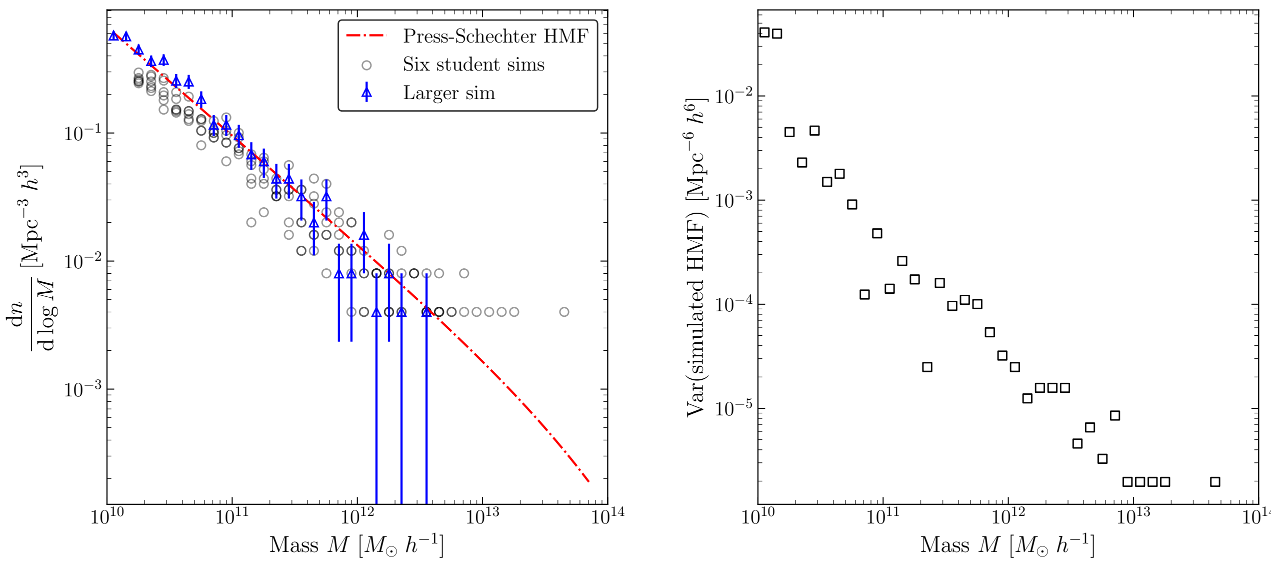

FIG. 4. HMF at $z = 0$ from six similarly initialised N-body simulations ($\ell_\mathrm{b} = 20$ Mpc and $\mathcal{N} = 64^3$) and one larger simulation ($\ell_\mathrm{b} = 40$ Mpc and $\mathcal{N} = 128^3$), compared to the theoretical HMF in the PS formalism. The five other sets of data points came from candidates 15001, 15002, 15004, 15008 and 15012. The right panel shows the variance of the data at each mass bin.

density maps visually confirm this bottom-up structure growth, evolving from a fairly homogeneous soup at high redshift to a cosmic web dominated by massive halos and filaments at $z = 0$. Finally, we see the local effect of this assembly in the shrinking spatial extent and increasing central density of the most massive halos, as they experience gravitational collapse and continued accretion.

B. DM halo density profiles

From our analysis of the density profiles, we find no evidence for cored density profiles in the simulated halos. The logarithmic slopes α of the averaged profiles, shown in Figure 3, provide the clearest evidence against this. We observe that $\alpha \to -1$ at small radii ($r \lesssim 10^{-1} R_\mathrm{vir}$), a characteristic signature of a central cusp that is inconsistent with a flat, constant-density core. The systematic flattening of the curves towards the center at lower redshifts does not indicate the formation of a core, but rather a steepening cusp, as the slope remains distinctly nonzero. Therefore, we conclude that the simulated halos maintain cuspy density profiles across the redshift range studied.

While the NFW profile was fitted to individual halos before averaging the resulting parameters, our analysis nevertheless reveals limitations in this approach. The failure to define a scale radius at $z = 2.984$, where the logarithmic slope never reaches $\alpha = -2$, indicates that the averaging process itself can obscure important physical characteristics. This demonstrates that the resulting average parameters, particularly the concentration values which show no clear evolutionary trend, may not reliably represent the underlying halo population.

We also note that the use of `pynbody` presented some challenges for the analysis. Its complicated and occasionally lacking documentation slightly inhibited the efficiency and the depth of the structural analysis, potentially introducing uncertainties in the profile extraction process.

C. Simulation accuracy and compliance with theoretical predictions

Overall, the N-body simulation provided accurate results and complied with our expectations. The density profiles of the largest DM halos followed the theoretical NFW profile, as seen in the assymptotic behaviour of the logarithmic slope α.

The HMF from our primary simulation shows strong agreement with the PS prediction, as quantitatively demonstrated by the high Pearson correlation coefficients of ~ 0.95 in log-space and statistically significant p-values of $p \lesssim 10^{-4}$. However, when considered collectively with the six other realisations, a more nuanced picture emerges. The ensemble of smaller-volume simulations reveals slight but systematic deviations from the theoretical HMF, exhibiting a deficit of halos at the low-mass end ($M \lesssim 10^{11} M_\odot h^{-1}$) and an excess at the high-mass end ($M \gtrsim 5 \times 10^{12} M_\odot h^{-1}$). This indicates that while the PS formalism accurately captures the global statistical behaviour, the finite box size of the smaller simulations introduces biases at the mass extremes.

The higher variance for low-mass halos also suggests that their abundance is more susceptible to cosmic variance or simulation-specific effects. In contrast, the low variance results for high-mass halos point to a more robust and universal prediction. This phenomenon can be explained intuitively; at the largest mass scales, we would expect to see a sharp cut-off in all the HMFs, since none of the simulations should have had enough time to form such massive halos (e.g. $M = 10^{14} M_{\odot} h^{-1}$) through gravitational collapse of already existing smaller halos. Meanwhile, at the lowest mass scales, we would expect that the appearance of new small DM would be subject to stochastic processes and thus exhibit a higher variance between the different realisations.

Furthermore, the larger-volume realisation of the simulation showed greater agreement with the PS HMF, especially at low mass scales. It would therefore be interesting to perform an even larger simulation with higher resolution in order to possibly resolve even smaller halos and thus probe the low-mass end of the HMF with higher precision.

VI. CONCLUSION

We have seen that this N-body simulation successfully demonstrated the hierarchical nature of cosmic structure formation in a Planck ΛCDM Universe. The evolution from a nearly homogeneous density field at $z \simeq 5$ to the intricate cosmic web observed at $z = 0$ provides clear evidence of bottom-up structure growth, where small-scale structures form first and subsequently merge into progressively larger systems.

The HMF analysis quantitatively confirms this hierarchical growth. The systematic migration of simulated data points down the PS curve with decreasing redshift demonstrates that halos continuously accrete mass over time. Strong correlation coefficients ($r \sim 0.95$, $p \lesssim 10^{-4}$) between our simulation and PS theory validate the fundamental predictions of hierarchical structure formation.

At the individual halo level, the shrinking spatial extent and increasing central densities of the most massive halos with decreasing redshift further illustrate ongoing gravitational collapse and continued accretion. The cuspy density profiles, with logarithmic slopes $\alpha \to -1$ at small radii and $\alpha \to -3$ at large radii, are consistent with the NFW profile predicted by collisionless dark matter simulations.

In conclusion, our simulation provides compelling evidence for hierarchical structure formation across multiple observables, from large-scale density distributions to the internal structure of individual dark matter halos.

[1] Sijing Shen. Lecture notes. Course: AST4320 Cosmology and Extragalactic Astronomy, 2025.

[2] Julio F. Navarro, Carlos S. Frenk, and Simon D. M. White. The structure of cold dark matter halos. *The Astrophysical Journal*, 462:563, May 1996.

[3] Oliver Hahn and Tom Abel. Multi-scale initial conditions for cosmological simulations: Multi-scale initial conditions. *Monthly Notices of the Royal Astronomical Society*, 415(3):2101–2121, July 2011.

[4] J.W. Wadsley, J. Stadel, and T. Quinn. Gasoline: a flexible, parallel implementation of treesph. *New Astronomy*, 9(2):137–158, February 2004.

[5] Steffen R. Knollmann and Alexander Knebe. Ahf: Amiga's halo finder. *The Astrophysical Journal Supplement Series*, 182(2):608–624, May 2009.

[6] A. Pontzen, R. Roškar, G. S. Stinson, R. Woods, D. M. Reed, J. Coles, and T. R. Quinn. pynbody: Astrophysics Simulation Analysis for Python, 2013. Astrophysics Source Code Library, ascl:1305.002.

Appendix A: Figures

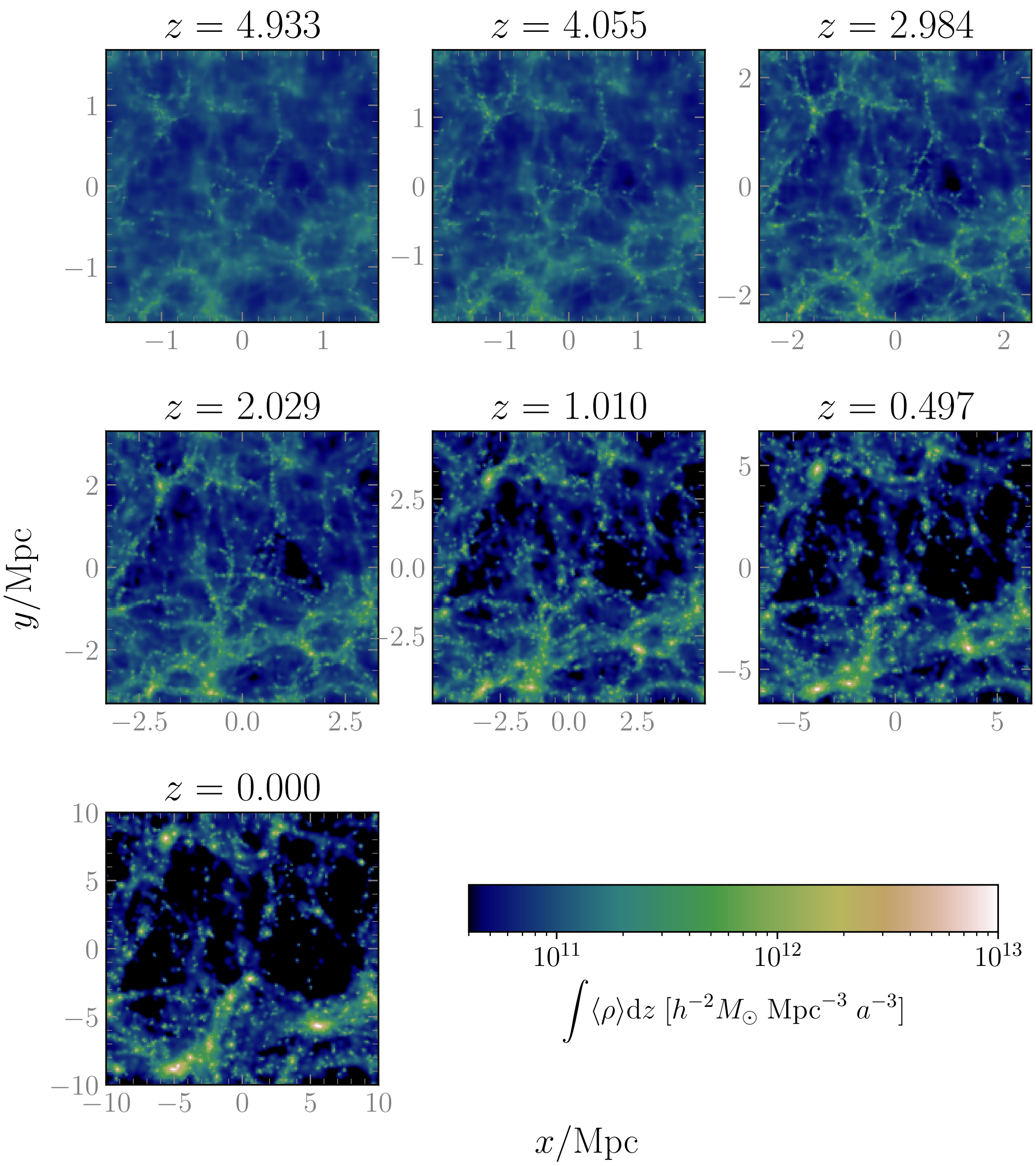

FIG. A1. Column density maps, for the whole simulation box, showing the DM in the snapshots at redshifts $z \simeq \{5, 4, 3, 2, 1, 0.5, 0\}$ projected along the x-axis.

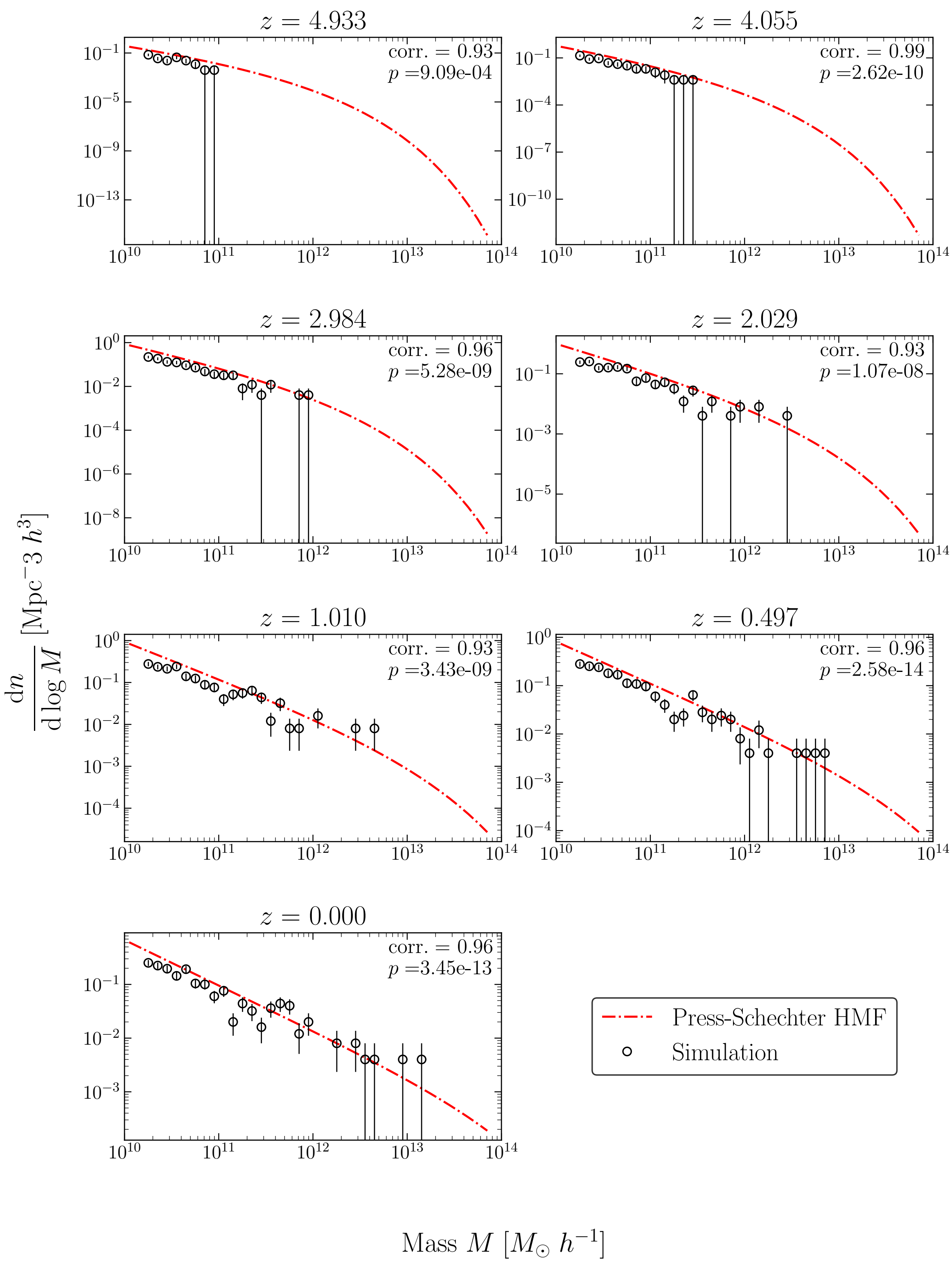

FIG. A2. Simulation HMF along with the theoretical HMF from the PS formalism at redshifts $z \simeq \{5, 4, 3, 2, 1, 0.5, 0\}$. In the top right of each panel, the Pearson correlation coefficient in log-space is indicated along with the corresponding p-value.